SABI 2011 IOP Publishing
Journal of Physics: Conference Series **332** (2011) 012022 doi:10.1088/1742-6596/332/1/012022

Estimation of electrical conductivity of a layered spherical head model using electrical impedance tomography

M Fernández-Corazza, N von-Ellenrieder and C H Muravchik
Laboratorio de Electrónica Industrial, Control e Instrumentación (LEICI)
Facultad de Ingeniería, Universidad Nacional de La Plata (UNLP), Buenos Aires, Argentina
E-mail: marianof.corazza@ing.unlp.edu.ar

Abstract. Electrical Impedance Tomography (EIT) is a non-invasive method that aims to create an electrical conductivity map of a volume. In particular, it can be applied to study the human head. The method consists on the injection of an unperceptive and known current through two electrodes attached to the scalp, and the measurement of the resulting electric potential distribution at an array of sensors also placed on the scalp. In this work, we propose a parametric estimation of the brain, scalp and skull conductivities using EIT over an spherical model of the head. The forward problem involves the computation of the electric potential on the surface, for given the conductivities and the injection electrode positions, while the inverse problem consists on estimating the conductivities given the sensor measurements. In this study, the analytical solution to the forward problem based on a three layer spherical model is first described. Then, some measurements are simulated adding white noise to the solutions and the inverse problem is solved in order to estimate the brain, skull and scalp conductivity relations. This is done with a least squares approach and the Nelder-Mead multidimensional unconstrained nonlinear minimization method.

1. Introduction

Electrical impedance tomography (EIT) is a relatively new imaging method that has evolved over the past 20 years. In the medical field it has a potential clinical value in diagnostics and monitoring of a number of disease conditions, from the detection of breast cancer [1], to monitoring brain function [2], and possibly stroke [3]. EIT consists on the injection of small electrical currents in different points of the body and the measurement of the resulting electric potential distribution through a sensor array. It is safe, portable, inexpensive and fast [4]. At present, EIT does not have the spatial resolution of other methods like Magnetic Resonance Imaging (MRI) or Computer Tomography (CT), while its key advantage is the temporal resolution, which is in the order of milliseconds [3].

In neuroscience, EIT can be used for at least two different applications: to image conductivity changes or to measure absolute conductivities. The former is based on measuring the conductivity changes produced by blood flow and volume alterations during evoked activity in the brain [4]. Also, a slight (∼1%) change of the impedance is produced in the cerebral cortex during neuronal depolarization [4]. But since the skull is more resistive than the other tissues of the head, the current that may reach the brain is relatively small [4] (less than 15% of total

injected current in a simulation study [5]). This is why in order to use EIT as a functional brain mapping tool, the shield effect of the skull to the injecting currents should be estimated first [6]. The second application is a technique for measuring the electrical conductivity of the head, useful to create an anatomical conductivity map. In this application, the EIT forward problem consists of computing the electric potential distribution generated by a known injected current in a known head model with its corresponding conductivity map. The EIT inverse problem is the estimation of the electric conductivity map from the electric potential measured at the electrode positions. As mentioned, the spatial resolution that can be achieved from EIT data alone is poor.

We propose to parameterize the inverse problem by a few parameters being the electric conductivity of the tissues, assuming the spatial distribution of the tissues is known. In this study, this spatial distribution consists of three concentric spheres. But next, realistic geometry obtained from some other techniques such as MR or CT scalp will be used. The approximate conductivity map will have then a very good spatial resolution but with conductivity values that may differ a little from the real ones since they are assumed homogeneous in each tissue. The proposed methodology is expected to work very well to estimate the scalp and skull conductivities, and a combination with some other techniques can complete the model. Diffusion Tensor Imaging (DTI) can be used to estimate the brain and cerebrospinal fluid (CFS) conductivities [7]. The knowledge of the conductivity map is important in the study of electroencephalography (EEG) problems, in particular for the estimation of the position of neural sources.

The EEG source localization problem aims to determine the neural sources inside the brain that best explain the electrical potentials measured on the surface of the scalp. The determination of the sources is made through the use of mathematical models which describe the head as an electrical conductor. Then, the knowledge of the electrical conductivity map of the head is important since it is known that the solution to the source localization problem is highly dependent on the values taken by the scalp, skull, and brain conductivities [8].

The scalp impedance plays a major role in head EIT, as it is engaged with currents of the highest density coming from the electrodes, and therefore it is the first stage in which distribution of current into the rest of the layers is determined. Any inaccuracies at this stage will substantially affect the impedance readings of the inner layers [9]. Several studies lead to a wide range of values (see Horesh graphs and tables [9]) showing the importance of *in vivo* and per patient based information. Regarding the skull, there are two kinds of mature bones: compact bone and spongy bone [9]. Many of the skull bones are flat, consisting of two plates of compact bone (thickness of 1.7 to 4.3 mm) enclosing a narrow layer of cancellous bone (thickness of 3.8 - 5.1 mm) containing bone marrow. Data published regarding skull impedance also covers a wide range of values. Dielectric properties of the skull are influenced by several factors: bone composition (skull layers-structure), non-uniform geometry, anisotropy and age (water content is reduced and bone marrow is changing from red to yellow with age, which decreases the conductivity) [9]. *In vivo* and per patient based information regarding the skull impedance is needed for building more accurate models to use in EEG and functional EIT problems.

In the next section we describe the adopted head model in detail. Then, we explain the mathematical background of the forward problem. Next, we state the inverse problem, and finally, the results of several simulations for different number of electrodes are presented and discussed.

2. Methods

2.1. Electrical Model

The head model consists of three concentric spherical shells with the enclosed space between them representing the three main tissues of the head: scalp, skull and brain (figure 1). Each layer

is considered as homogeneous and isotropic, i.e. conductivity is constant and with no preferred direction.

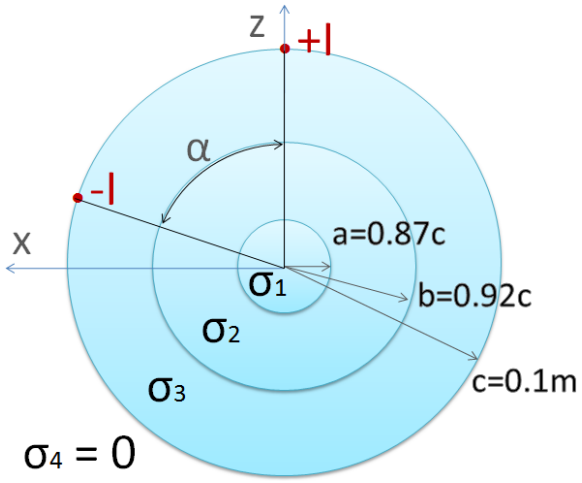

Figure 1. Electrical model. σ_1, σ_2 and σ_3 represent homogeneous and isotropic conductivities of brain, skull and scalp respectively. $+I$ and $-I$ represent the positive and negative current injection points.

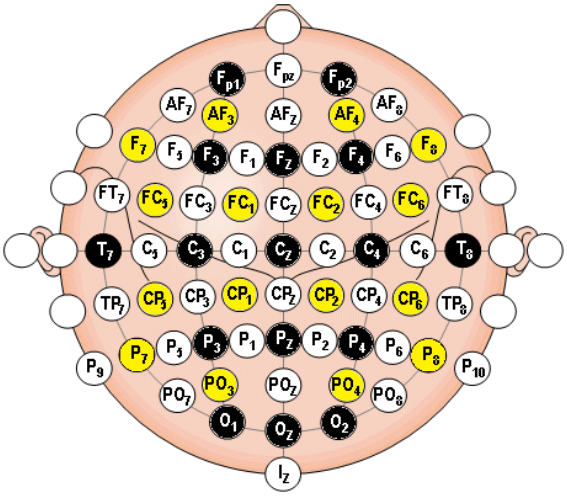

Figure 2. Electrode positions based on the 10-10 system over a spherical head. Black, black and shaded, and labeled circles show the positions used for 16, 32 and 64 configurations respectively.

The electrode placement used is based on the 10-10 system for 64, 32 and 16 sensors (figure 2). A pair of electrodes is selected for the current injection, while the others are dedicated to measure the resultant electric potential difference. One of the current electrodes will supply a current of $+I$ (current source) and the other a current $-I$ (current sink), both with the same absolute value (figure 1).

EIT applications usually comply with the International Electrotechnical Commission (IEC) standard [10] which specify a "patient auxiliary current" limit of $100\mu A$ from 0.1 Hz to 1 kHz. This standard is based on limitation of the current to 10 % of the average threshold of sensation when current is applied to the skin using surface electrodes. This corresponds to a widely cited study in which a mean perception current of 1.1 mA was observed between DC and 200 Hz, for hand holding of a copper wire of d = 3.3 mm in diameter [11]. This gives a threshold current density around 2 to 15 A/m^2. In another study ([12]), with abrasion just under a conventional cup electrode (Ag/AgCl, 11 mm diameter), the threshold of sensation was $100 - 200\mu A$ and it became slightly unpleasant at $400\mu A$. This gives a threshold current density similar to previous study. Then, a current of $100\mu A$ is appropriate for use in real studies with patients. We use this value to produce a realistic simulation.

Also, the model dimensions must be scaled to a human head. So, the outer shell radius is set to $10cm$. The other radii are the ones that are mostly used in spherical models [13]. Table 1 summarizes the interface radii chosen for the model.

The remaining data to complete the model are the isotropic conductivity values. These are found in the literature with a high dispersion (table 2 shows some examples). Some of them are measurements and some others are reference values given in the studies. The values chosen for the present work are shown in the last row. The criteria was to select realistic values, with two exact decimals for brain:skull and brain:scalp conductivity ratios in order to ease the comprehension of the results.

Table 1. Model radii

Interface	Label	Radius [cm]
Brain:Skull	a	10.0
Skull:Scalp	b	9.7
Scalp:Air	c	8.7

Table 2. Conductivity values found in literature [S/m]

Author	Brain	Skull	Scalp
Zheng Xu et al [6]	0.33	0.04	0.33
Gilad et al [12]	∼0.30	0.015	∼0.30
Abascal et al [5]	0.30	0.039	0.44
Adhazi et al [14]	0.25	0.018	0.44
Gonçalves et al [8]	0.33	0.008	—
Horesh [9]	0.15	0.02	0.25
Liston et al [15]	0.25	0.018	0.44
Zlochiver [16]	0.12 (grey matter)	0.02 (bone)	0.35 (muscle)
Fernández-Corazza	0.30	0.01	0.40

2.2. Forward Problem

Assuming that the scalp, skull, and brain conductivities are known, the problem consists on estimating the electric potential on the outermost surface. This is an electromagnetism problem with surface conditions and spherical geometry. Maxwell equations govern the physics of electromagnetism. In particular, for low frequencies, the quasi-static assumption can be used. This is common in many studies since it reduces the complexity of the problem [3]. The limitation is that the model is valid only for frequencies below ∼10 kHz, for which the wave length is much greater than the head dimensions. Then, we can write

$$\vec{\nabla} \times \vec{E} = 0, \tag{1}$$

where $\vec{E}$ is the electric field. From (1), the electric field $\vec{E}$ can be expressed as the gradient of a scalar potential Φ

$$\vec{E} = -\vec{\nabla}\Phi. \tag{2}$$

It is known that the current density $\vec{J}$ is proportional to $\vec{E}$ (3) [17].

$$\vec{J} = \sigma\vec{E}, \tag{3}$$

Where, σ is the electric conductivity of the medium. Applying the divergence to $\vec{J}$ and assuming that σ is constant,

$$\vec{\nabla} \cdot \vec{J} = \vec{\nabla} \cdot (\sigma\vec{E}) = \sigma(\vec{\nabla} \cdot \vec{E}) = \sigma(-\vec{\nabla}^2\Phi). \tag{4}$$

The current conservation law states that the divergence of the current density is zero everywhere in the sphere except in the injection points. With this approximation, the electric potential Φ must satisfy the Laplace equation in each layer:

$$\vec{\nabla}^2\Phi = 0. \tag{5}$$

Taking advantage of the problem symmetries, for each layer i, the solution of the potential Φ in every point of the space (r,θ,ϕ) can be expressed as a linear combination of the Legendre Polynomials as shown in (6) [17] [18].

$$\begin{aligned}\Phi^{(i)}(r,\beta,\gamma) &= \sum_{l=0}^{\infty}(A_l^{(+)(i)}r^l + B_l^{(+)(i)}r^{-l-1}).P_l(cos\beta) - \sum_{l=0}^{\infty}(A_l^{(-)(i)}r^l + B_l^{(-)(i)}r^{-l-1}).P_l(cos\gamma)\\ \Phi^{(i)}(r,\beta,\gamma) &= \sum_{l=1}^{\infty}(A_l^{(i)}r^l + B_l^{(i)}r^{-l-1}).(P_l(cos\beta) - P_l(cos\gamma)); \qquad i=1,2,3. \end{aligned} \tag{6}$$

Where the constants $A_l^{(i)}, B_l^{(i)}$ depend on the boundary conditions, $P_l(x)$ is the Legendre Polynomial of order l (where $P_0(x)=1$), $\beta(\theta,\phi)$ is the angle to the $+I$ current source and $\gamma(\theta,\phi)$ to the $-I$ current sink. In layer 3, the potential is not exactly as (6) because the current injection points are within this layer and their effect must be included. Applying linearity, the potential on this layer can be expressed as the potential in an unbounded medium (Φ_{unb}) plus another with the expression of (6) ($\Phi^{(3)}$) that allows the total potential on this layer ($\Phi_{tot}^{(3)}$) to satisfy the boundary conditions. Then,

$$\Phi_{tot}^{(3)} = \Phi_{unb} + \Phi^{(3)}, \tag{7}$$

where,

$$\Phi_{unb} = \frac{I}{4\pi\sigma_3}\left(\frac{1}{\sqrt{r^2+c^2-2rc.cos(\beta)}} - \frac{1}{\sqrt{r^2+c^2-2rc.cos(\gamma)}}\right). \tag{8}$$

Note that the constant $B_l^{(1)}$ must be zero in order to have continuity at the origin. So, for each order l, there remain five constants $A_l^{(1)}, A_l^{(2)}, B_l^{(2)}, A_l^{(3)}, B_l^{(3)}$ to be determined. On the interface between the layers, two conditions are satisfied: the continuity of the normal components of the current density and the continuity of the electric potential. They lead to five equations:

$$\begin{aligned}\sigma_1\frac{\partial\Phi^{(1)}}{\partial r}\bigg|_{r=a} &= \sigma_2\frac{\partial\Phi^{(2)}}{\partial r}\bigg|_{r=a}\\ \sigma_2\frac{\partial\Phi^{(2)}}{\partial r}\bigg|_{r=b} &= \sigma_3\frac{\partial\Phi_{tot}^{(3)}}{\partial r}\bigg|_{r=b}\\ \sigma_3\frac{\partial\Phi_{tot}^{(3)}}{\partial r}\bigg|_{r=c} &= 0\\ \Phi_1|_{r=a} &= \Phi^{(2)}\Big|_{r=a}\\ \Phi_2|_{r=b} &= \Phi_{tot}^{(3)}\Big|_{r=b}\end{aligned} \tag{9}$$

Solving the equation system derived from (9) the constants can be determined. Then, expanding and regrouping terms, the potential over the outermost surface ($r=c$) can be written as:

$$\Phi_{tot}^{(3)}(c,\theta,\beta) = \frac{k}{c}.\left(\Phi_\infty + \sum_{l=1}^{\infty}\left(\frac{K_1.\sigma_1/\sigma_2 + K_2.\sigma_1/\sigma_3 + K_3.\sigma_2/\sigma_3 + K_4}{K_5.\sigma_1/\sigma_2 + K_6.\sigma_1/\sigma_3 + K_7.\sigma_2/\sigma_3 + K_8} - 1\right).(P_l(cos\beta) - P_l(cos\gamma))\right), \tag{10}$$

where,

$$k = \frac{I}{4\pi\sigma_3}, \tag{11}$$

$$\Phi_\infty(\beta,\gamma) = \frac{1}{\sqrt{|2-2\cos(\beta)|}} - \frac{1}{\sqrt{|2-2\cos(\gamma)|}}, \tag{12}$$

$$K_1 = (l+1+lb_r^{2l+1})l(1-(a_r/b_r)^{2l+1}), \tag{13}$$

$$K_2 = (1-b_r^{2l+1})l(l+(l+1)(a_r/b_r)^{2l+1}), \tag{14}$$

$$K_3 = (1-b_r^{2l+1})l(l+1)(1-(a_r/b_r)^{2l+1}), \tag{15}$$

$$K_4 = (l+1+lb_r^{2l+1})(l+1+l(a_r/b_r)^{2l+1}), \tag{16}$$

$$K_5 = l^2(l+1)(1-(a_r/b_r)^{2l+1})(1-b_r^{2l+1}), \tag{17}$$

$$K_6 = (l+(l+1)(a_r/b_r)^{2l+1})(l^2+(l^2+l)b_r^{2l+1}), \tag{18}$$

$$K_7 = (l+1)l(1-(a_r/b_r)^{2l+1})(l+(l+1)b_r^{2l+1}), \tag{19}$$

$$K_8 = (l+1)l((l+1)+l(a_r/b_r)^{2l+1})(1-b_r^{2l+1}). \tag{20}$$

With a_r and b_r being the a and b radii relative to a sphere of radius 1, (i.e., $a_r = a/c$ and $b_r = b/c$).

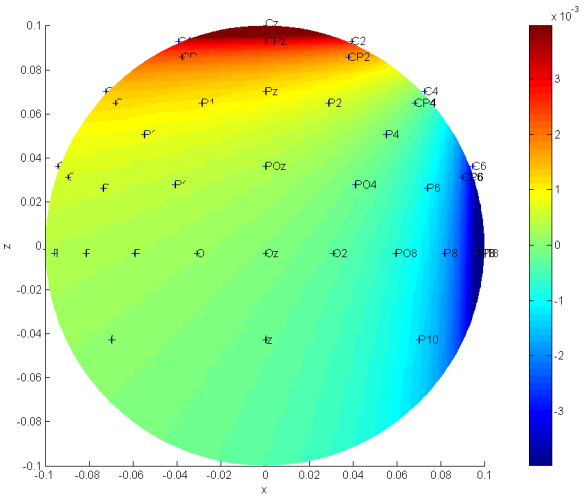

Figure 3. Surface potential for $\sigma_2 = 0.0093 S/m$, as seen from behind. The positions and labels for 64-electrode configuration are also displayed

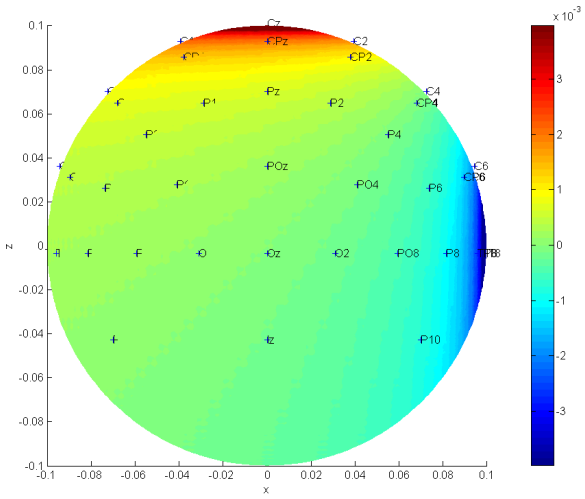

Figure 4. Surface potential for $\sigma_2 = 0.039 S/m$, as seen from behind. The positions and labels for 64-electrode configuration are also displayed

Figures 3 and 4 show the resulting electric potential Φ over the sphere surface for two different skull conductivity values. It can be seen that it changes with that parameter.

2.3. Inverse Problem

For the inverse problem the conductivities are assumed unknown, and the electric potential measured at the electrodes is known. In order to simulate the measurements, white gaussian noise is added to the solution of the forward problem with the previous section formulas (assuming the conductivities of table 2). This noise models the electronic noise of the amplifiers and the skin/electrode contact electrochemical noise. We model it as Gaussian distributed zero mean and $1\mu A$ standard deviation.

We will estimate the conductivity ratios instead of the conductivities themselves. This is convenient, for example, in (10). But only two of them are independent, so $x_1 = {}^{\sigma_1}/_{\sigma_2}$ and $x_2 = {}^{\sigma_1}/_{\sigma_3}$ are chosen as the independent variables implying that ${}^{\sigma_2}/_{\sigma_3} = {}^{x_2}/_{x_1}$.

Then, a least squares approach can be used to estimate the unknowns x_1 and x_2 that minimize the difference between each sensor measurement and its corresponding forward solution:

$$\min_{x_1,x_2} \left\{ \sum_{i=1}^{(n-2)} \left(V_i - \Phi\left(\theta_i, \beta_i, x_1, x_2\right)\right)^2 \right\}, \tag{21}$$

Where, n is the number of electrodes, V_i is the "measured" potential on the electrode i and $\Phi\left(\beta_i, \gamma_i, x_1, x_2\right)$ is the surface potential function obtained from the forward problem (10). The upper limit of the summation is $(n-2)$ because the injection nodes are excluded since their potential is not measured.

The optimization algorithm used is the Nelder-Mead multidimensional unconstrained nonlinear minimization method [19]. Note that in the formulation (21) there is a constrain (the unknowns must be positive), but as the starting point can be chosen relatively near to the true value, a faster unconstrained method can be used.

3. Results

The inverse problem (21) was solved for 16, 32 and 64 electrodes with $1\mu A$ standard deviation noise. It can be seen in figure 2 that there is a symmetry on the electrode distribution between left an right sides. This symmetry does not exist between front and back because of the three occipital electrodes (Iz, P9 and P10) in the 64-electrode configuration, and the Oz electrode in the 32 and 16 configurations. So, all different pairs of electrodes without an exact mirrored configuration occurring on the left side were considered. For example, the problem with the injection nodes being C4 and F4 leads to the exact same results of the C3-F3 combination. Then, this last pair was excluded. The number of combinations used are shown in table 3.

Table 3. Injection node combinations

Electrodes	Combinations
64	1551
32	391
16	99

For each combination, 100 different noise realizations were simulated and the mean and variance of the x_1 and x_2 estimates were computed. Figures 5 and 7 show, for the 64 and 32 electrode configurations, the mean of x_1 as a function of the angle α between the injection electrodes. The expected value is also displayed with a horizontal line. Figures 6 and 8 show the same results for x_2.

Figure 9 shows, for the 16-electrode configuration, the mean and mean plus/minus variance of the x_1 estimation for different combinations of injection electrodes. A particular injection pair has a very high variance. This is reasonable since it corresponds to the T7-T8 combination. In this case all measurement electrodes are close to the middle plane between these two positions, where the electric potential is close to zero.

Figure 11 shows the resulting variance for different x_1 simulations. Each cross represents the mean variance for each pair of injection electrodes. The central mark is the median, the edges

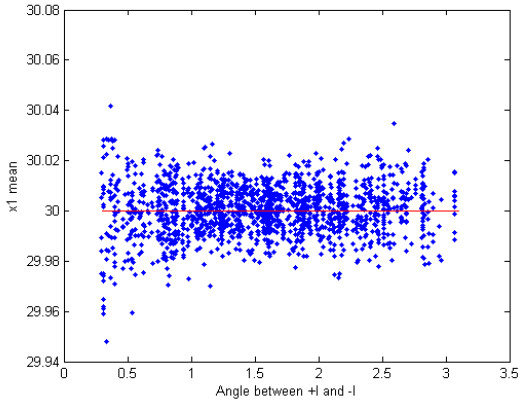

Figure 5. σ_1/σ_2 mean versus α for 64 electrode configuration.

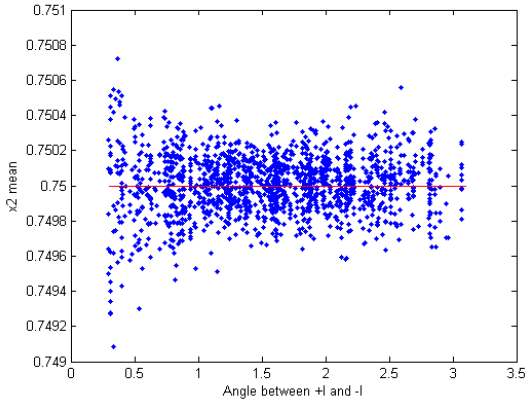

Figure 6. σ_1/σ_3 mean versus α for 64 electrode configuration.

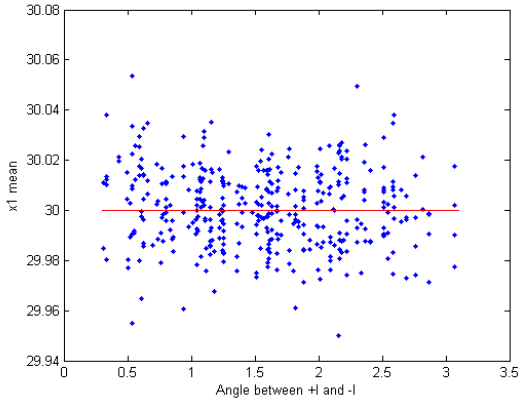

Figure 7. σ_1/σ_2 mean versus α for 32 electrode configuration.

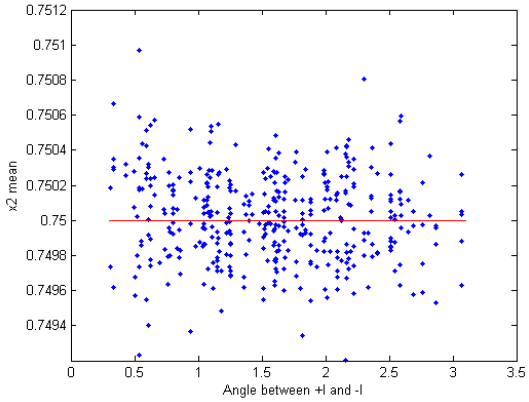

Figure 8. σ_1/σ_3 mean versus α for 32 electrode configuration.

of the box are the 25th and 75th percentiles, and the whiskers extend to the most extreme data points not considered outliers. Figure 12 shows the same result for x_2. The combination T7-T8 was excluded from both plots in the 16-electrode configuration because, as explained before, it is a very atypical case and would impact negatively in the plot readability.

Another simulation was done in order to study the impact of the assumed noise variance. We know that the brain has normal activity that can be detected with the EEG electrodes. This activity means for this application of EIT additional noise with peaks of around $20\mu V$. Although this noise might be disaffected using a proper technique (taking advantage of the fact that the frequency and phase of the injected current is well known), is important to know if such a technique effort is worthwhile. Then, the same simulation for 64 electrodes was ran, but with a noise standard deviation of $10\mu V$. Figure 10 compares the 16 and 64 electrode configurations with $1\mu V$ and $10\mu V$ of noise standard deviation respectively, where the left box of the plot is the same than the right one of figure 11.

4. Conclusions

The forward and inverse problems have been solved successfully for 16, 32 and 64 electrodes over the three shell spherical model and the expected conductivity values were retrieved. It is

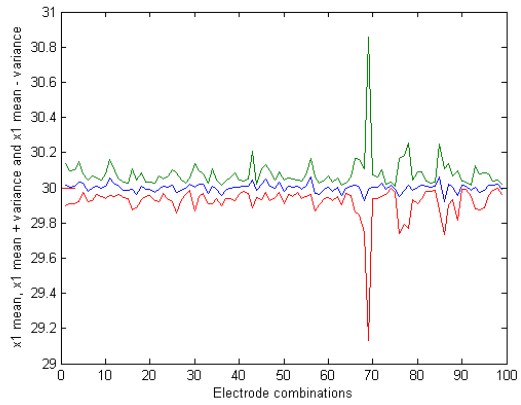

Figure 9. σ_1/σ_2 mean and mean plus/minus variance for 16-electrode configuration versus electrode combinations

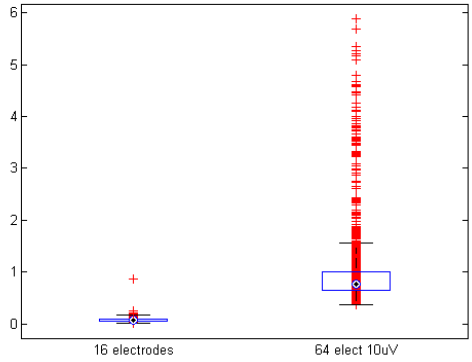

Figure 10. Box plot of the variance for σ_1/σ_2 estimations in 16 and 64 electrode configurations with $1\mu V$ and $10\mu V$ standard deviation noise respectively.

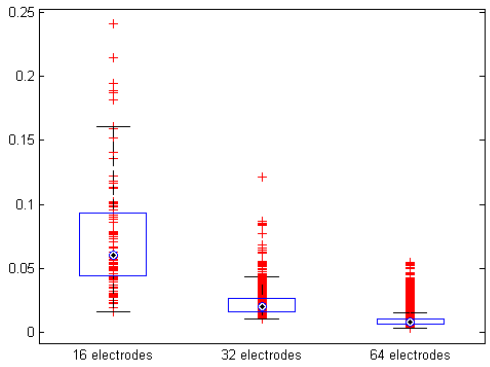

Figure 11. Box plot of the variance for σ_1/σ_2 estimations.

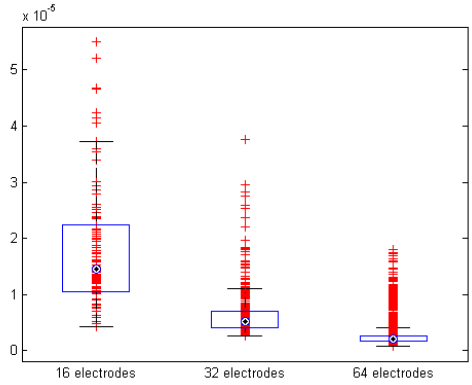

Figure 12. Box plot of the variance for σ_1/σ_3 estimations.

important to highlight that this was achieved with appropriate scales. For instance, the radius of the outer sphere was 10cm, close to a real head size. Also, the injected current value was chosen with the same criterion as if it were a real experiment. Furthermore, the conductivity values were close to real values, and finally, a typical electronic noise standard deviation was chosen.

Injection nodes with greater angle between them generally achieve better results (less variance) but this is not a general rule, since the accuracy not only depends on that angle, but also on the surrounding electrodes for measurement. For example, C3-C4 combination is better than T7-Cz (less variance), although both have very similar angle between the injection nodes. Another example is the atypical T7-T8 pair for the 16 electrode configuration, where the angle α between the electrodes is maximum and the variance of the conductivity estimation is the highest. In conclusion, the combinations with more sensors surrounding the injection electrodes and a large angle between them are preferred.

On the other side, the results show an exponential-like dependence of the variance with the number of electrodes. Of course, more electrodes mean better results, but from this study, and

also depending on the measurement precision needed, a good choice on the sensors quantity could be performed. More important than the amount of electrodes is the removal of the brain activity from the recorded signals. A cap with 16 electrodes and a system to remove the background brain activity is much better than a 64 electrodes system without it.

The spherical model mainly serves as a validation tool for numerical algorithms since the forward problem has analytical solution. With numerical methods like Boundary Element Method (BEM) or Finite Element Method (FEM), the algorithms can be independent of the geometry. The solutions for the forward and inverse problems with a real shaped model using FEM are in progress. This model will use a standard shape model of the head and a standard averaged conductivity distribution of the brain and CFS obtained via DTI. Then, it will be used to estimate the conductivities of skull and scalp. An advantage of using FEM instead of BEM is the possibility of include anisotropy in the model. It is known that skull has a tangential to radial anisotropy of around 1:10 [13]. The same seems to happen in the scalp, but in this case the relation is lower (1:1.5) [9] and it is not so relevant. So, the inverse problem will be extended to look for four unknowns: tangential skull, radial skull, tangential scalp and radial scalp conductivities.

The development of an EIT device is also planned. Using the average head model or patient specific models (if possible) jointly with this device, real estimations of scalp and skull conductivities will be performed. Since this information will be used to solve the EEG source localization problems, the real impact of having patient specific conductivity maps will be studied.

Acknowledgments

This work was supported by ANPCyT PICT 2007-00535, UNLP I127, CONICET and CICpBA.

References

[1] Cherepenin V A, Karpov A Y, Korjenevsky A V, Kornienko V N, Kultiasov Y S, Ochapkin M B, Trochanova O V and Meister J D 2002 *IEEE Trans. Med. Imaging* **21**(6) 662–667
[2] Bagshaw A P, Liston A D, Bayford R H, Tizzard A, Gibson A P, Tidswell A T, Sparkes M K, Dehghani H, Binnie C D and Holder D S 2003 *NeuroImage* **20** 752–764
[3] Bayford R 2006 *Annu. Rev. Biomed. Eng.* **8** 63–91
[4] Holder D 2008 *Automation Congress, 2008. WAC 2008. World* pp 1 –6
[5] Abascal J F, Arridge S R, Atkinson D, Shindmes R, Fabrizi L, Lucia M D, Horesh L, Bayford R H and Holder D S 2007 *Neuroimage* **43**(2) 258–68
[6] Xu Z, He W, He C, Zhang Z and Liu Z 2008 *Automation Congress, 2008. WAC 2008. World* pp 1 –5
[7] Tuch D S, Wedeen V J, Dale A M, George J S and Belliveau J W 2001 *Proceedings of the National Academy of Sciences of the United States of America* **98**(20) 11697–11701
[8] Gonçalves S I, de Munck J C, Verbunt J P A, Bijma F, Heethaar R M and da Silva F L 2003 *IEEE Trans. Biomed. Eng.* **50**(6) 754–767
[9] Horesh L 2006 Ph.D. thesis University College London
[10] IEC60601 2005 *Medical electrical equipment - part 1: general requirements for basic safety and essential performance* ed3.0 (Geneva: International Electrotechnical Commission)
[11] Dalziel C F 1972 *IEEE Spectr.* **9**(2) 41–50
[12] Gilad O, Horesh L and Holder D S 2007 *Med. Bio. Eng. Comput.* **45** 621–633
[13] Rush S and Driscoll D 1968 *Anasthesia and analgetica* **47**(6) 717–723
[14] Ahadzi G, Gilad O, Horesh L, Bayford R and Holder D S 2004 *ICEBI'04 - V Electrical Impedance Tomography* 621–624
[15] Liston A D, Bayford R H, Tidswell A T and Holder D S *Physiol. Meas.* **23** 105–119
[16] Zlochiver S 2005 Ph.D. thesis Tel Aviv University
[17] Jackson J D 1975 *Classical Electrodynamics Second Edition* (New York: John Wiley & Sons)
[18] Frank E 1952 *Journal of applied physics* **23**(11) 1225–1228
[19] Lagarias J C, Reeds J A, Wright M H and Wright P E 1998 *SIAM Journal of Optimization* **9**(1) 112–147